ORIGINAL ARTICLE

Improving surface integrity by optimizing slide diamond burnishing parameters after hard turning of 42CrMo4 steel

Jawad Zaghal[1] · Viktor Molnár[2] · Márton Benke[1]

Abstract

Despite turning could be replaced by grinding as a finishing machining process, it is considered not satisfactory for elongating the fatigue life of the component because of the produced tensile residual stresses and irregularities formed at the surface. Therefore, a complimentary operation should be applied after hard turning. Slide diamond burnishing process is a mechanical finishing operation used after hard turning to further decrease the surface roughness, introducing compressive residual stresses, increasing the microhardness, and refining the microstructure of the surface and subsurface layer of the workpiece. The main result is increasing the fatigue life of the rotating components subjected to cyclic loading. In this work, the simultaneous effect of changing the burnishing speed, feed, and force of slide diamond burnishing on surface roughness, residual stresses, and microhardness of 42CrMo4 hard-turned steel was studied. It was found that the effect of one parameter was highly affected by the others. As a result, the optimal burnishing parameters were specified, with which better surface quality was obtained than after grinding.

1 Introduction

Nowadays, hardened steels find extensive application in the automobile sector, namely for the production of pinions, camshafts, crankshafts, and crown wheels. Since these parts usually work under dynamic loading circumstances, their fatigue strength should be of high level [1]. When the hardness of such parts exceeds 45 HRC, their machining is described as hard [2, 3]. Since precision hard turning has the ability to replace traditional grinding in machining hardened components, its usage in the industrial sector has expanded dramatically [4]. However, later it was found that hard turning does not provide sufficient surface finish or proper hardness in the subsurface layers and can result in tensile residual stresses, having unfavorable effects on fatigue life span.

Thus, to overcome these limits of hard turning, a finishing operation, like slide diamond burnishing (SDB), is required after hard turning to obtain proper surface integrity.

SDB is a finishing process that resembles turning kinematically but without chip removal, in which a deforming tool with a spherical end-usually made of natural or synthetic diamond-moves under pressure over the surface of the workpiece, causing plastic deformation and, hence, a minute material flow on the surface and a mirror-like appearance [5, 6]. The main merits of the process are improving the corrosion and wear resistance, increasing the microhardness, decreasing the surface roughness, inducing compressive residual stresses, and refining the microstructure of the surface. As a result of that, the fatigue strength of the workpiece will be improved [5]. These advantages make it possible to substitute grinding by SDB of hard-turned steel components [6].

Both conventional and CNC lathe machines are mostly used for performing the burnishing process. As the workpiece rotates, the burnishing head is forced against it and moves axially. The basic controlling parameters of the SDB process are the burnishing force (F_b, N), burnishing feed (f, mm/rev), rotational speed of the component (n, rpm),

✉ Jawad Zaghal
jawad_za@ppu.edu

[1] Institute of Physical Metallurgy, Metalforming and Nanotechnology, University of Miskolc, Egyetem Út 1, Miskolc 3515, Hungary

[2] Institute of Manufacturing Science, University of Miskolc, Egyetem Út 1, Miskolc 3515, Hungary

or the burnishing speed (v, m/min), and the deforming head radius (r, mm).

So far, many studies have been conducted to investigate the influence of burnishing parameters and their interactions on the outputs of the burnishing process, like surface roughness, surface residual stresses, microhardness, and microstructure. The results of those studies show that the efficacy of the burnishing process highly depends on the range of the applied burnishing parameters and their interactions, the type of burnished material and its hardness, and the environment of the burnishing process, like lubrication and wear of the burnishing head.

For example, to investigate the effect of the SDB process on the resultant surface roughness, Ra, in a research conducted by Liska et al. [7] on 36 surfaces made of 100Cr6 steel with a hardness of 64 HRC, values of Ra changed from 0.291, 0.39, 0.885, and 2.168 μm after the hard turning, to 0.118, 0.167, 0.153, and 1.24 μm after burnishing with different burnishing settings, respectively. Kluz et al. [5] performed another recent work on 42CrMo4 steel shafts with a hardness of 22 HRC and a turning surface roughness Ra of 2.6 μm. There were 11 burnished surfaces in all, with Ra values varied between 0.137 and 0.225 μm. In a third investigation, Tobola et al. [8], on AISI D2 steel of 60 HRC hardness, he was able to lower the turned surface roughness Ra from 0.82 to 0.24 μm after burnishing. In another example, using eight turned surfaces of Vanadis 6 powder metallurgy steel of 61 HRC hardness, Brostow et al. [9] found that the surface roughness Ra was reduced from 0.97 μm after turning to a range begins with 0.18, 0.26, up to a maximum roughness of 0.41 μm. The last example is the study of Huuki and Laakso [10]. They have succeeded in reducing Ra from 1.78 μm after turning to 0.39 μm after burnishing, carried out on 34CrNiMo6-M steel with a hardness of 30 HRC.

Concerning the impact of the process on the improvement of surface residual stresses, for instance, in a study accomplished by Okada et al. [11] using AISI 316 stainless steel with a hardness of 200 HV, after the burnishing process, stresses in the axial direction were in the range of 320 to -300 MPa and from 400 to -800 MPa in the tangential direction. In another investigation carried out by Maximov et al. [12] using annealed samples made of 41Cr4 steel, the output axial stresses were about -700 MPa, while tangential stresses were around -350 MPa. The third example is of a research accomplished by Konefal et al. [13]. The study was carried out on austenitic X6CrNiMoTi17-12-2 alloy steel. After burnishing, the axial stresses were -918 MPa and the tangential ones were -501 MPa. Lastly, in a study carried out using 42CrMo4 steel with a hardness of 32 HRC by Korzynski et al. [14], only the axial stresses were measured because, according to the author, they play a significant role in improving the fatigue life of the rotating shafts and axles. The results were between -145 and -461 MPa.

The third important result of the burnishing process that was studied by researchers is the improvement of surface microhardness. Raising a surface's hardness primarily serves to increase its resistance to wear [15]. In the study of Toboła et al. [16] carried out on Vanadis 6 and D2 steels of hardness ≈ 60 HRC, the increment of microhardness after burnishing was 10%. In another research done by Maximov et al. [17] on D16T aluminum alloy used in the aircraft industry, with a hardness of 110 HB, they improved the microhardness of the surface by 36% using one SDB pass and 50.4% using seven passes. Another examples is an investigation conducted by Łabanowski et al. [18] using UNS S32550 duplex steel with a hardness of 270 HV0.2. In this work, the highest enhancement of the microhardness was 70.3% with a cold worked layer of 1020 μm. The final case is about a study in which the goal of using the SDB process was to improve the structure and properties of the surface layer of the detonated coated parts of the gas turbine made of Kh12NMBF-Sh (ÉP-609) steel, done by Boguslaev et al. [19]. For some parts burnished with specific parameters, their microhardness has increased by about twice as much as their starting value.

The previously mentioned examples show that the range of the results and improvements is wide and strongly depends on the different parameters of the SDB process, the burnished metal, and its hardness. One of the main shortages in the studies that have been carried out on the topic of SDB so far is that feed and burnishing force are the two most researched variables, but fewer have checked the effect of burnishing speed. Moreover, there is a dearth of publications that concurrently analyze the resultant roughness, microhardness, and residual stresses [17]. Consequently, in the current study, the effect of changing the burnishing speed, feed, and force simultaneously has been studied. Furthermore, their influence on surface roughness, residual stresses, and microhardness after the burnishing process has been examined.

In addition, all prior SDB investigations using 42CrMo4 steel had hardness values lower than 33 HRC [5, 14, 20–23]. However, in this study, the burnishing process was accomplished after the hard turning of cylindrical bars of 54 HRC hardness since this steel grade is primarily intended to be hard-turned in some applications [24, 25]. Consequently, this work contributes to the slide burnishing operation on this grade of steel in its hardened state.

2 Experimental setup

2.1 Material and specimens preparation

The main goal of this research is to increase the surface quality of rotating workpieces. It is well known that fatigue

Table 1 Chemical composition of AISI 4140 steel (wt%) [27]

C	Si	Mn	P	S	Cr	Mo	Ni	V
0.38–0.45	0.17–0.37	0.5–0.8	0.035 max	0.035 max	0.9–1.2	0.15 – 0.25	0.3 max	0.06 max

Table 2 Mechanical properties of AISI 4140 steel [5]

Yield stress $R_{p0.2}$, MPa	Ultimate tensile stress Rm, MPa	Elongation, %	Hardness, HB	Toughness KV, J
650	900–1100	12	265–325	Min. 35 at 20 °C

Table 3 Burnishing parameters experimental design matrix

Surface no	F_b [N]	f [mm/rev]	v [m/min]
1	50	0.03	41
2	100		
3	150		
4	50	0.06	
5	100		
6	150		
7	50	0.09	
8	100		
9	150		
10	50	0.03	82
11	100		
12	150		
13	50	0.06	
14	100		
15	150		
16	50	0.09	
17	100		
18	150		
19	50	0.03	115
20	100		
21	150		
22	50	0.06	
23	100		
24	150		
25	50	0.09	
26	100		
27	150		

happens in the rotating parts due to fluctuating or repetitive stresses [26], in which surface quality plays a key role. Therefore, it is essential that the selection of steel grade be relevant to the purpose of this study. As a result, the steel grade 42CrMo4 (AISI 4140) was chosen according to its applications. In addition, thisgrade can be hardened up to 54–55 HRC, which is in the range where the turning can be considered hard. The chemical composition of this steel can be seen in Table 1 [27], and Table 2 shows its basic mechanical properties [5]. Specimens are in the form of bars of 50 mm in diameter and 200 mm in length. Each bar was sectioned into six surfaces of 25 mm in length, with a 5 mm distance between each section or surface. Workpieces were then austenitized at 855°C, quenched in oil, and tempered for two hours at 240°C to a hardness of 54 HRC.

After hardening, the hard turning was performed on an OPTIturn S 600 CNC lathe using an insert from Mitsubishi Materials Company, model number: CNGA120408TA4 MB8025. The cutting speed (v_c) was 120 m/min, the cutting feed (f) was 0.1 mm/rev, the tool nose radius (r_ε) was 0.8 mm, and the depth of cut (a_p) was 0.2 mm.

2.2 Burnishing conditions

Samples were burnished using three levels of force (F_b), feed (f), and speed (v). The combinations of burnishing parameters are shown in Table 3. As can be seen, the total number of surfaces is 27, which is considered a high number when compared to some studies in the literature, which were carried out using eleven or even fewer surfaces. This point has the advantage of covering a wide range of possible combinations of the three parameters.

Burnishing was done using an EU-400-01 universal lathe and a burnishing tool with a 3 mm radius tip made of PCD (polycrystalline diamond) manufactured at the Institute of Manufacturing Science at the University of Miskolc. According to the results of the study done by Nestler and Schubert [28], this radius value could improve the surface roughness resulting from the SDB process. Burnishing was carried out using SAE 15W-40 oil.

2.3 Measuring surface roughness, surface residual stresses, and microhardness

The arithmetic mean surface roughness (Ra) of the burnished pieces was measured using the AltiSurf 520 device. In those measurements, the measurement length was 1.5 mm in the axial direction, the evaluation length was 1.25 mm, and the cut-off was 0.25 mm. These parameters were chosen in accordance with ISO 21920-2:2021 for roughness measurements. For each surface, 3 measurements were taken at equal angles (120°) at the perimeter, and the average value was calculated.

Surface residual stress components of the two main directions were measured, namely the tangential (speed) and axial (feed) directions. The $sin^2\psi$ method was used with a Stresstech G3R type centerless diffractometer, equipped with

a Cr X-ray source. For measurements, the {211} reflections were measured. During the measurements, a collimator of 2 mm in diameter was utilized. The tilting positions were 5 in both tilting directions (left and right) with maximum tilting angles of $\mp 45°$. Exposure time was chosen to be 4 s. Background extraction was done using linear subtraction, and the material parameters were Young's modulus and Poisson's ratio. For each surface, 3 measurements were taken at equal angles (120°) at the perimeter, and the average was calculated.

Surface microhardness was measured using the device model Wilson Instruments, Tukon 2100 B. The Vickers microhardness was measured at three different points at the top of each surface using a 200-g load, and then the average value was calculated.

3 Results and discussion

As was mentioned above, a comprehensive study was conducted on the effects of different burnishing parameters on the surface roughness, surface residual stresses in the axial and tangential directions, and the microhardness. Table 4 shows the numerical results, and the analytical results for each measured parameter will be discussed in detail.

The standard deviations of the data were calculated for each level of the burnishing parameters and for all the data points, and the results are summarized in Table 5. The standard deviations increase as a function of the burnishing force, except in the case of Ra, it decreased. The standard deviation of the Ra increases, those of the axial residual stress and the hardness decrease as a function of the feed rate, and there is no clear tendency in the case of the tangential residual stress. The standard deviations of the residual stresses increase as a function of the burnishing speed, and there is no clear tendency in the cases of the Ra and the HV 0.2 parameters.

3.1 Results of surface roughness *Ra*

The initial surface roughness before the SDB process has a great influence on the resultant roughness of the burnished surface [29–31]. It is worthwhile to mention that the surface roughness after turning was 0.2 μm, which is considered a good value to be followed by SDB. The results of Ra after burnishing are shown in Fig. 1. For convenience, the chart shows the burnishing parameters for each surface, keeping in mind, as mentioned in Table 3, that three forces were used with each feed: $F_1 = 50N$, $F_2 = 100N$, and $F_3 = 150N$.

Numerous inferences can be made from this chart. It can be seen that the majority of the burnished surfaces have a better surface roughness than their previous turned state (before burnishing). The best three surfaces in terms of Ra are surfaces 19, 24, and 20, respectively. Despite

**Table 4** Results of surface roughness, surface residual stresses, and microhardness

Surf. no	Ra [μm]	σ-axi [MPa]	σ-tan [MPa]	HV 0.2
Turned	0.2	−41	662	631
1	0.134	−1032	−542	721
2	0.151	−1167	−607	719
3	0.204	−1313	−623	778
4	0.167	−1011	−510	675
5	0.172	−1033	−623	707
6	0.201	−1130	−660	661
7	0.202	−987	−447	675
8	0.147	−964	−551	652
9	0.159	−1005	−641	660
10	0.144	−986	−511	698
11	0.154	−1157	−503	703
12	0.311	−968	−304	950
13	0.186	−982	−448	667
14	0.175	−1160	−579	735
15	0.533	−1134	−289	939
16	0.144	−896	−488	698
17	0.137	−980	−634	700
18	0.603	−757	−311	816
19	0.125	−905	−500	696
20	0.131	−1203	−633	723
21	0.475	−843	−133	891
22	0.191	−1068	−603	713
23	0.134	−1285	−725	747
24	0.129	−1278	−706	734
25	0.252	−1013	−475	677
26	0.234	−1084	−563	688
27	0.621	−873	−181	740

Table 5 Standard deviation results of the responses

	Level	Ra [μm]	σ-axi [MPa]	σ-tan [MPa]	HV 0.2
F_b [N]	50	0.0405	55.8	48.5	18.7
	100	0.0320	107.1	63.3	27.9
	150	0.1988	193.9	226.6	110.5
f [mm/rev]	0.03	0.1174	154.5	164.7	93.0
	0.06	0.1236	109.1	137.9	84.1
	0.09	0.1939	95.9	150.3	50.3
v [m/min]	41	0.0261	112.2	70.2	40.8
	82	0.1805	132.3	125.0	108.7
	115	0.1767	168.6	212.8	63.5
All data		0.1473	137.7	151.9	79.5

the fact that many researchers have mentioned that speed has a minor effect on the results of the burnishing process [9, 21, 28, 32], it is clear that the combination of burnishing force and speed has a major effect on the results

Fig. 1 Results of Ra, axial and tangential surface residual stresses after burnishing. $v_1 = 41$, $v_2 = 81$, $v_3 = 115$ [m/min]. $f_1 = 0.03$, $f_2 = 0.06$, $f_3 = 0.09$ [mm/rev]
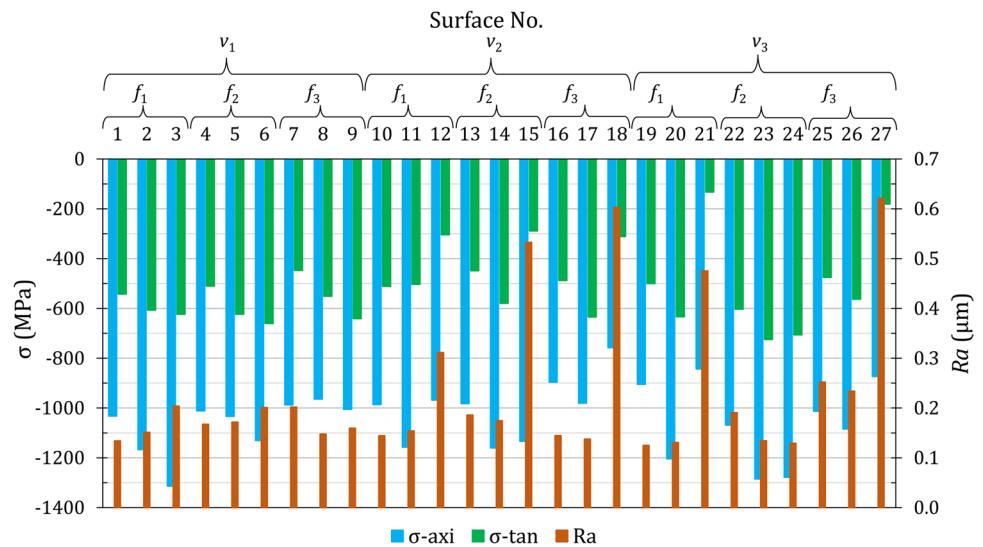
of surface roughness. The majority of surfaces burnished with the first speed v_1 are smoother than the turned ones. Of those surfaces, six have a smaller roughness than the turned state, and the rest three are equal to it. Also, for the surfaces burnished with the first and second feeds (f_1 and f_2), as the burnishing force increases, the resultant surface roughness increases too. Additionally, the values of Ra with f_1 are less than f_2 because, according to the relationship between the burnishing parameters [33]:

$$L = f \times n \times t \qquad (1)$$

where L is the burnished length, [mm], f is the burnishing feed, [mm/rev], n is the burnishing speed, [rpm], and t is the burnishing time, [min]. As the burnishing feed increases, the burnished length increases too, and then Ra increases, since the distances between ridges and valleys on the burnished surface increase too. The same result was found by Nestler and Schubert [28]. Moreover, the general trend in these first six surfaces is that as burnishing force increases, the resultant Ra increases too. The reason for that may refer to the fact that in this range of the parameters, when increasing the force, the contact pressure will increase, and that leads to scaling of the surface caused by the material fatigue, which finally leads to an increment in the surface roughness [28, 34].

Moving on to the surfaces that were burnished with the second and third velocities (v_2 and v_3), they have eleven surfaces with Ra less than the turned state, and seven greater. Among those seven surfaces, five of them were burnished with the highest force (F_3). These high values of Ra mostly happened because of the combined effect of the high speed, which, according to Eq. (1), increases the surface roughness, and the effect of the high force, which could degrade Ra as discussed before. Nevertheless,

this combined effect did not affect the surface number 24, which means that the combined effect of the three burnishing parameters (v_3, f_2 and F_3) is different in this case. In conclusion, the interaction between burnishing parameters depends on the range in which those parameters interact, especially the speed and force.

For a comprehensive understanding of the relationship between the three burnishing parameters and their effect on the surface roughness Ra, the 3D representation shown in Fig. 2 summarizes the correlation between them. It is clear from the figure that there are two trends. The first trend is when using the first and second forces, F_1 and F_2. The second trend is when using the third force, F_3. In the case of using F_1 and F_2, the effect of changing the burnishing speed and feed on Ra is not that huge, and the results are interchangeable. In the case of F_1, values range from 0.125 to 0.25 μm, while with F_2 they lie in the range between 0.13
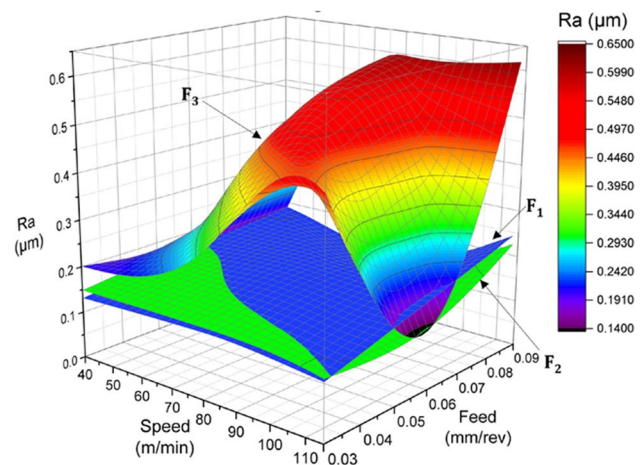

Fig. 2 The relationship between Ra and the burnishing parameters

and 0.23 μm. On the other hand, the range of Ra results when F_3 was used is between 0.13 and 0.62 μm.

It can also be seen that the best results of Ra when F_1 is used could be achieved using v_1 or v_3 with f_1, and when F_2 is used, the best surface roughness could be acquired using v_3 with f_1 or f_2. Finally, the best value of Ra could be achieved by utilizing v_3 with f_2 when the third force, F_3, is being used. Conversely, a highly rough surface could be yielded when applying F_3 with v_2 and f_1 or f_3, or v_3 with f_3, or their surroundings.

3.2 Results of axial and tangential surface residual stresses

Generally speaking, inducing compressive residual stresses on the surface of the component is considered an improvement to the surface, which could enhance the fatigue life [35]. They can delay or prevent the development and propagation of cracks, thereby increasing the service life of mechanical components [36]. Thus, as is evident, investigating the generated surface residual stress after the process of SDB is of great importance. Therefore, residual stresses at the surface of the burnished surfaces were measured in two important directions: the axial (feed) and tangential (speed). Figure 1 reveals the average values of those stresses for the whole surfaces. It's important to know that the axial stresses after turning were -41 MPa and the tangential were 662 MPa.

Many findings can be drawn from the chart. First of all, stresses in both directions are compressive, and in the axial direction they are greater than those in the tangential one, which has a significant influence on improving the fatigue life of the component since the introduced residual stresses by the burnishing process in the axial direction have the greatest improvement effect on the fatigue life of axes and shafts exposed to cyclic bending [32]. In the axial direction, the lowest three values are -757, -843, and -873 MPa for surfaces 18, 21, and 27, respectively. On the other hand, the three highest values are -1313, -1285, and -1278 MPa for surfaces 3, 23, and 24, respectively.

In addition, for the first speed, with f_1 and f_2, as the burnishing force increases, the axial stresses increase too, but the results with f_1 are greater than with f_2, but with f_3 a slight drop happens with F_2, and the changes are minor. Another important remark is that, for the surfaces burnished with velocities v_2 and v_3, the whole surfaces that were burnished using F_2 have higher axial stresses than those that were burnished with F_1 or F_3, regardless of the burnishing feed. Moreover, the surfaces that were burnished with the third speed v_3 have axial stresses greater than those that were burnished with the second speed v_2 and with the same feed and force, except for the pairs (10, 19) and (12, 21). Finally, using the same feed and force, the surfaces that were

burnished with v_1 have axial stresses that are greater than or close to those that were burnished using v_2, except for the pair (5, 14).

Moreover, when the first speed v_1 was used, a direct relationship between the burnishing force and the resultant tangential stresses can be seen, regardless of the burnishing feed. Whereas, from surface number 12 to surface number 27, the case is different; the lowest tangential stresses are for the surfaces burnished with the third force F_3, and the highest stresses are for the surfaces burnished with the second force F_2, while the surfaces burnished with the first force F_1 have midrange values, regardless of the burnishing speed and feed. What can also be noted is that, from surface 12 to 20, as the burnishing force changes from F_3 to F_1 to F_2, stresses increase linearly.

The reason for this arrangement (relationship between force and stress) is that the first force, F_1, is not high enough to produce a contact pressure that is able to produce high compressive stresses in the burnished layer, but this is not the case with F_2. Whereas, the third force, F_3, is too high; therefore, material fatigue results in scaling at the surface layer, which allows for stress relaxation. The same happened with Nestler and Schubert [28]. This relationship is obvious in the same figure, which shows the relationship between the absolute values of surface residual stresses and surface roughness Ra. Stresses and roughness are clearly seen to be in harmony from surface 1 to 6, neutral from 7 to 11, and completely opposite from 12 to 27.

The opposing connection between stresses and roughness in the domain of surfaces 12 and 27 is because more roughness indicates larger scaling and irregularities, which leads to greater stress relaxation. It is highly noted that the surfaces with higher roughness were burnished with the maximum force, F_3. However, since the speed and feed were changed, the roughness levels were also varied. Kuznetsov et al. [29] also showed in their study that high forces could destroy the surface after SDB. Nevertheless, burnishing speed and feed play a significant role in determining the consequent value of surface roughness, even when using F_3, as seen by the low roughness and significant residual stresses on the 24_{th} surface, although it was burnished using F_3.

Now, to get a thorough understanding of the interactions between burnishing parameters and their effect on the resulting axial surface residual stresses, the whole results were gathered in the 3D illustration shown in Fig. 3. It is clear that the burnishing force has great influence, and the behavior of each force (surface) is different and highly depends on the value of the burnishing speed and feed. The best compressive stresses could be achieved using F_2, then F_3 with some speeds and feeds, and finally F_1. With F_1, stresses range between -900 MPa with v_2 and f_3 and -1070 MPa with v_3 and f_2. When F_2 was used with v_1 and f_3, the lowest (less compressive) stress value was -960 MPa, and the highest
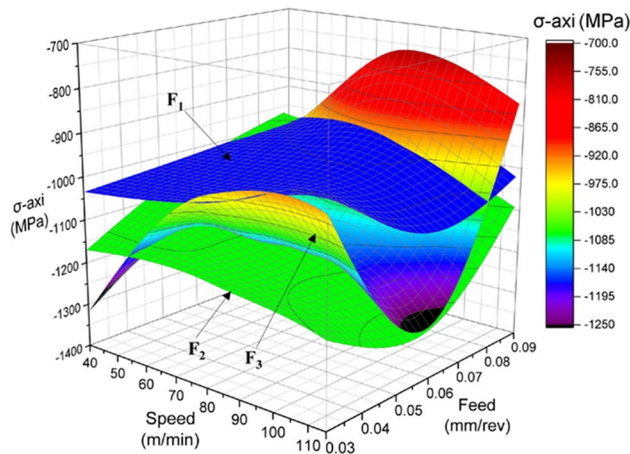
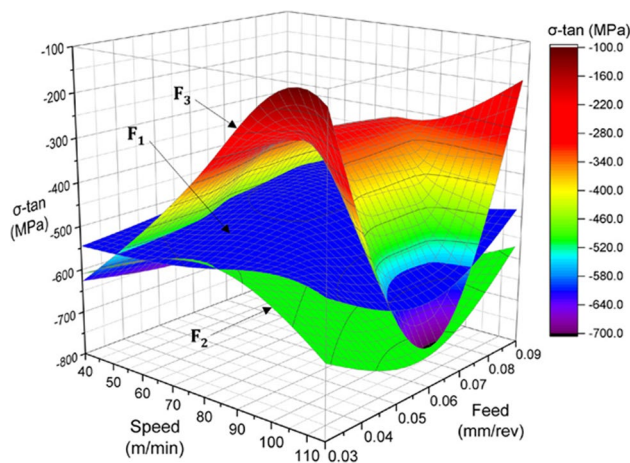**Fig. 3** The relationship between axial residual stresses and the burnishing parameters

Fig. 4 The relationship between tangential residual stresses and the burnishing parameters

stress value was -1285 MPa with v_3 and f_2. In the case of F_3, -760 MPa was the lowest stress value with v_2 and f_3, and -1315 MPa was the highest when v_1 and f_1 were used.

On the other hand, the 3D representation of the effect of burnishing parameters on the tangential surface residual stresses can be seen in Fig. 4. Again, we can clearly see the effect of the burnishing force. If we compare the effect of forces between the axial and tangential cases, we can see that the output tangential stresses when using F_1 and F_2 are much closer than in the case of axial stresses. In addition, the effect of F_3 is totally different in the two directions. In the case of axial direction, the majority of stresses using F_3 are more compressive than in the case of using F_1, except in the case of burnishing at high feeds. Whereas, in the tangential direction, the majority of stresses generated by F_3 are less compressive than those generated by F_1, except when using low speeds and using v_3 with f_2.

In the tangential direction, the lowest compressive stress generated by F_1 is -450 MPa when it was used with v_1 and f_3, and the maximum is -600 MPa when this force was used with v_3 and f_2. When F_2 was used, -500 MPa was the lowest compressive stress when v_2 and f_1 were used, and -725 MPa was the highest with v_3 and f_2. Finally, -133 MPa was the lowest stress value when F_3 with v_3 and f_1 were used, whilst -705 MPa was the highest compressive stress when F_3 was used in combination with v_3 and f_2. In the end, changing the level of burnishing parameters will totally affect the resulting surface stresses in the axial and tangential directions, and the effect of one burnishing parameter depends on the other parameters, as well.

Improving the fatigue life of a component requires not only improving the surface layer integrity but also improving the subsurface layer [12, 32, 37]. Inducing compressive residual stresses is a key component of subsurface layer improvement factors. As the depth of this layer increases, the fatigue life of the component will also increase [36]. Because of this, it is very important to measure the depth of the burnished layer to find out how different burnishing parameters, especially force, affect the beneficial zone of compressive stresses.

Figures 5 and 6 show the axial and tangential residual stress distributions (depth profiles) for three surfaces that were burnished with the three levels of the force and have the lowest surface roughness values and with high surface compressive residual stresses. The samples are 19, 20, and 24, burnished with 50, 100, and 150 N, respectively. The effect of the burnishing process in generating the compressive residual stresses zone is obvious when comparing the depth profiles of the samples after burnishing with the turned one. Again, in depth, axial residual stresses are greater than stresses in the tangential direction.

In both charts, one might easily deduce that the effect of the burnishing force is of great influence. The 50 N force has generated the lowest compressive stresses with a beneficial zone of about 135 µm, which is considered a significant depth. Furthermore, despite the fact that the compressive residual stresses at the surface of the sample burnished with 100 N are lower than those at the surface of the sample burnished with 150 N, the situation is reversed beneath the surface. The compressive stresses produced by the 100 N force under the surface are greater than those generated by the 150 N one, especially in the axial direction, with an effective compressive zone of 140 µm. The reason for that may refer to the fact that the high forces may cause the nucleation of microcracks under the burnished layer when locally exceeding the strength of the surface layer. The same happened with Tobola et al. [37] when they applied 180 N of burnishing force with a feed of 0.02 mm/rev on Vanadish 6 steel bars of 60 HRC.

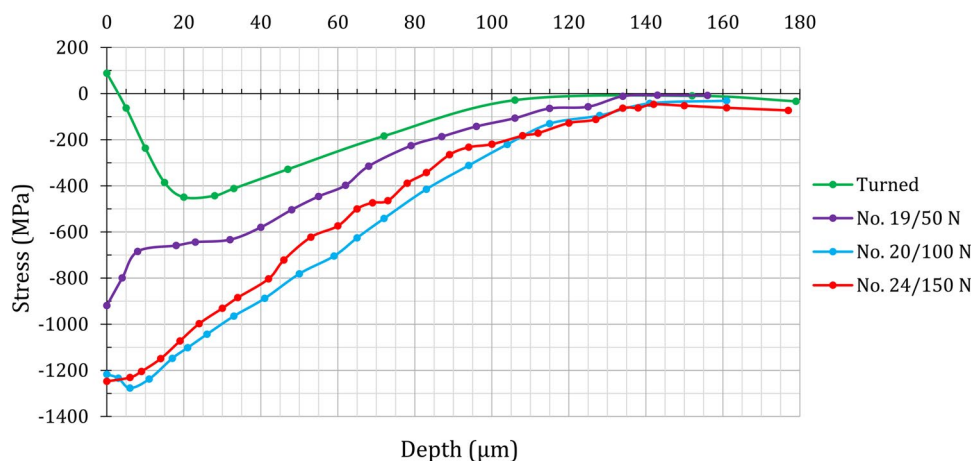**Fig. 5** Axial stresses depth profiles after turning and burnishing of specific surfaces
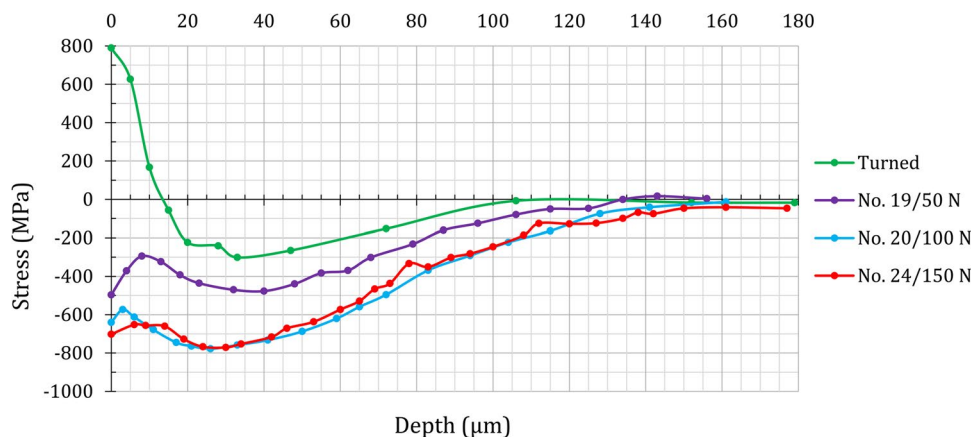

Fig. 6 Tangential stresses depth profiles after turning and burnishing of specific surfaces

3.3 Results of microhardness

One of the main purposes of the SDB process is to increase the surface microhardness of the burnished component. It is mainly accomplished by grain refinement and increasing the density of dislocations via strain hardening [38]. The microhardness of the burnished surfaces was also measured to assess the effect of the different burnishing parameters and their interactions. The results of Vickers microhardness testing of the surface of the burnished workpieces and their percentages of improvement can be seen in Fig. 7. To facilitate the comparison, microhardness after turning (before burnishing) has also been shown.

It can be seen that the hardness of the entire surfaces has improved, but to varying degrees and depending on the speed at which forces were applied. When the first speed v_1 was used, the effect of the burnishing force was not huge and not constant, and, in general, the results of microhardness were reduced as the burnishing feed was raised. With this speed, the best result was achieved when F_3 was used with f_1.

Whereas, in the case of using the second speed, v_2, it can be seen that, among the whole 27 samples, the highest improvements were attained using this speed with the highest force, F_3. With this speed, the increment in microhardness between using F_1 and F_2 was not that big, but a significant increment happened when F_3 was used, especially with the lowest feed, f_1, then with f_2, and finally with f_3.

Eventually, in the case of using the highest speed, v_3, the highest improvements were obtained using F_3 with f_1, then F_2 with f_2, and finally, F_3 with f_3. Evidently, with f_1 and f_3, as the burnishing force increases, the percentage of microhardness increases too. In conclusion, we can deduce that the best results of microhardness improvements could be obtained when the highest force, F_3, is used with the lowest feed, f_1, and v_2, then with v_3, and finally with v_1.

Now, for a comprehensive presentation of the effect of changing the three burnishing parameters together, the 3D representation of that relationship is depicted in Fig. 8. It is shown that, in general, as the burnishing force increases, the resultant microhardness increases too. The difference in results between surfaces burnished with F_1 and F_2 is marginal, but a significant change appeared when F_3 was used. In the case of using F_1 or F_2, the influence of changing the burnishing speed or feed is not significant, whereas in the case of utilizing the highest force, F_3, we can see a substantial impact of the speed and feed. The best

Fig. 7 Results of surface micro-hardness and their percentages of improvement after burnishing. $v_1 = 41$, $v_2 = 81$, $v_3 = 115$ [m/min]. $f_1 = 0.03$, $f_2 = 0.06$, $f_3 = 0.09$ [mm/rev]
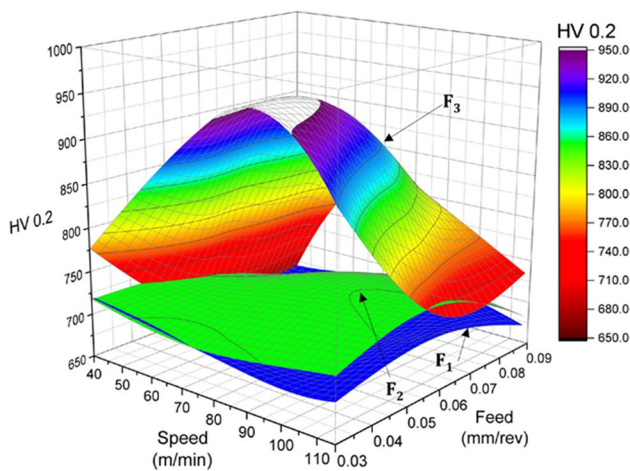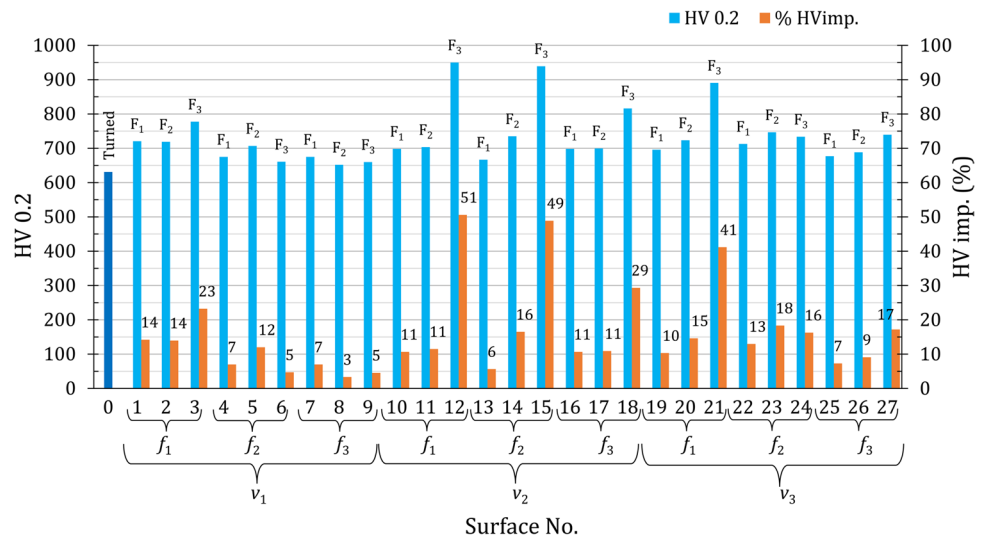

Fig. 8 The effect of changing burnishing parameters on microhardness

superior outcomes could be reached when F_3 used with the midrange speed, v_2, and the lowest feed, f_1. In short, it's not enough to just study the effect of changing one burnishing parameter while leaving the others unchanged. It's also important to see how changing the other parameters affects the one that's being studied.

3.4 Analysis of surface morphology and topography

When the surface quality gets better, there are fewer places where cracks can start [18]. The surface morphology and 3D topography for surfaces 19, 20, and 24 after burnishing have been examined and shown in Fig. 9. The 3D surface topography of the surfaces before burnishing (after turning) is shown as well.
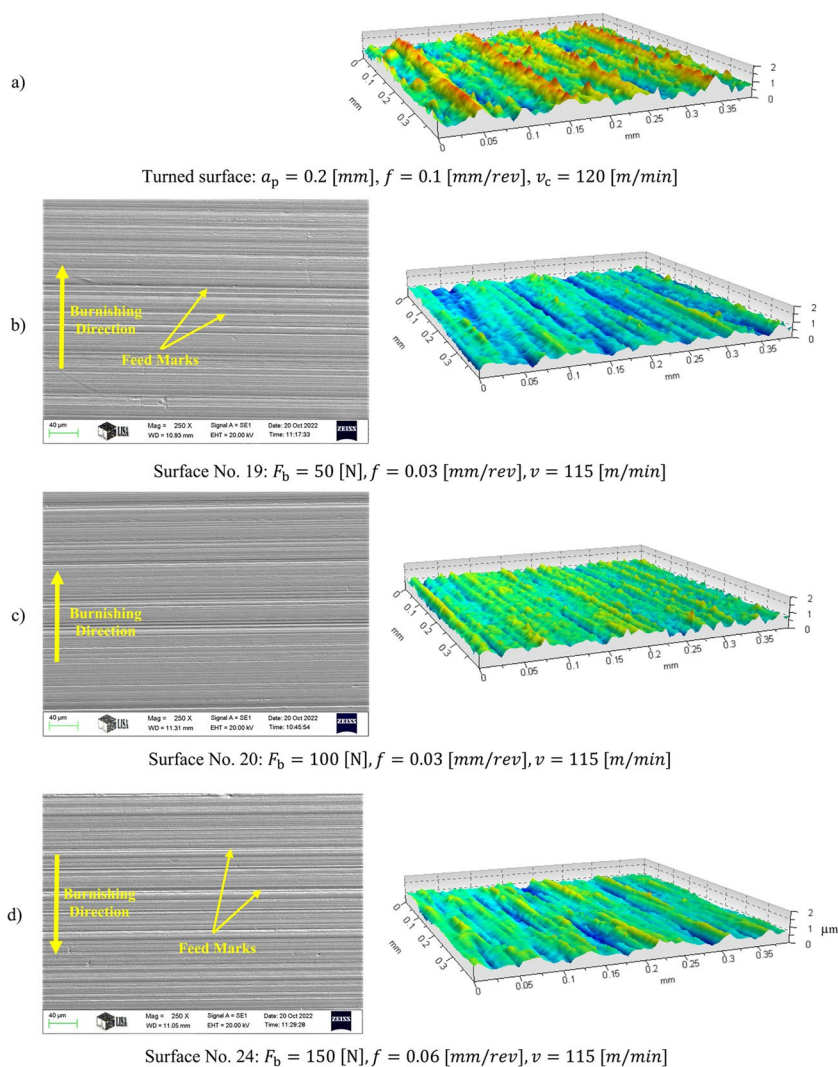
From the 3D patterns, one can clearly see that the surface structure after turning is full of sharp peaks. However, those burrs are less noticeable after burnishing than they are after turning. Moreover, the peak-to-valley distance is substantially reduced after burnishing than after turning, and the ridges and valleys are more rounded after burnishing because the radius of the burnishing tool head is higher than that of the turning cutting tool.

Likewise, the SEM surface topography micrographs show the effect of the burnishing parameters on the surface structure. The effect of the burnishing feed is evident; surfaces 19 and 20 were burnished with 0.03 mm/rev feed, while surface 24 was burnished with 0.06 mm/rev feed. It can be clearly seen that the feed marks are much less visible on the surfaces burnished with the lower feed than on the one with the higher feed. Lastly, the final geometrical structure of a surface is quite sensitive to the burnishing force used. Inevitably, as the burnishing head advances, surface irregularities will undergo plastic deformation. In the case of surface 19, the force was not enough to suppress the peaks that resulted from turning and to generate a regular, uniform surface profile when compared to surface 20. Whilst, with surface 24, the high contact pressure caused by the burnishing force was sufficient to swell and flow the surface material, leaving behind both consecutive fine and coarse traces.

3.5 Analysis of cross-sectional microstructure

In order to investigate the effect of the burnishing process and its parameters on the surface microstructure, cross-sectional SEM micrographs were taken for samples 19, 20, and 24 as shown in Fig. 10. The plastic deformation of the surface grains is pretty obvious. Clearly, one may see that the deformed, burnished grains are more compacted than the in-depth ones. Additionally, the burnishing force is the dominant factor in this case. Mainly,

Fig. 9 The effect of increasing burnishing force and feed on surface morphology and topography

a)

Turned surface: $a_p = 0.2 \, [mm], f = 0.1 \, [mm/rev], v_c = 120 \, [m/min]$

b)

Surface No. 19: $F_b = 50 \, [N], f = 0.03 \, [mm/rev], v = 115 \, [m/min]$

c)

Surface No. 20: $F_b = 100 \, [N], f = 0.03 \, [mm/rev], v = 115 \, [m/min]$

d)

Surface No. 24: $F_b = 150 \, [N], f = 0.06 \, [mm/rev], v = 115 \, [m/min]$

it affects the depth of the deformed layer and the compactness of the deformed grains. The conclusion is obvious: for surface 19, the burnishing force was the lowest; therefore, the effect of plastic deformation was not so high, and the maximum depth of the deformed layer is not more than 3 μm. Whereas, in the case of surface 20, which was burnished with a higher force, the influence is more evident, with a distorted depth of about 5 μm. Finally, since the surface 24 was burnished with the highest force, approximately, the whole grains along the burnishing line were deformed. They are more compacted than the previous surfaces, and the impact of the burnishing process reached a deeper distance. It is approximately 7 μm thick.
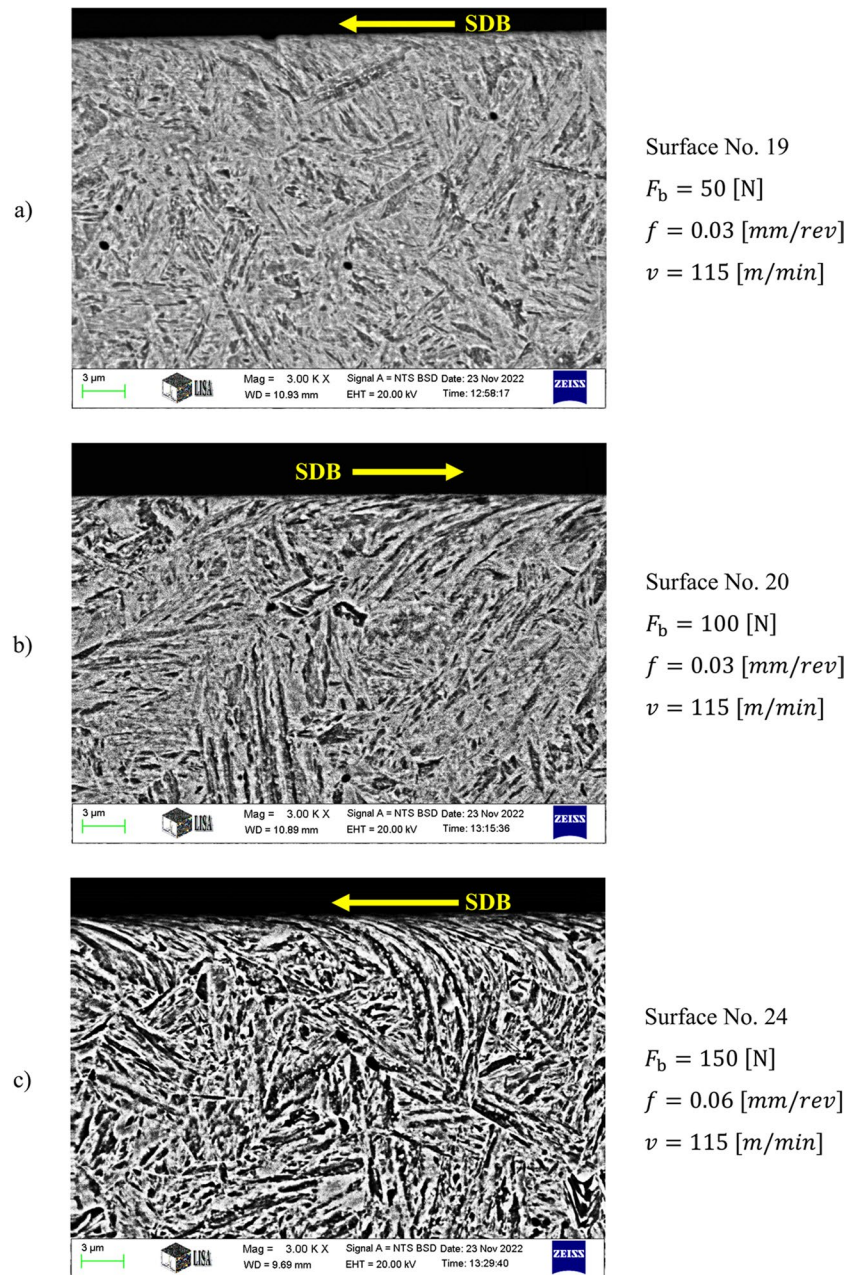
3.6 Statistical analysis

Statistical analytics were carried out to explain the effects of influencing factors, i.e., the burnishing parameters (independent variables) on the analyzed response values, i.e., *Ra* roughness, axial and tangential residual stresses, and HV 0.2 hardness (dependent variables). To determine if the variation of the values of a dependent variable results from the values of an independent variable or the interaction of more than one independent variable, analysis of variance (ANOVA) is suggested to be carried out. The numerical results of it provide information about the clearly influencing factors [40]. If there is no connection (the null hypothesis is fulfilled), the source of variation is due to random phenomena [39].

To carry out an ANOVA analysis, the distributions of the groups, among which the analysis is intended to be carried out, should be normal or at least symmetric. To analyze this preliminary condition, Shapiro-Wilk tests were carried out for each dependent variable, which were grouped based on each corresponding independent variable. In this test, the P-value of a group should be higher than a critical value (decision: accept normality). The number of elements (of a group) was nine, and the critical value (significance level)

Fig. 10 Cross-sectional micro-structure SEM micrographs of specific surfaces after burnishing with different forces

Surface No. 19
$F_b = 50$ [N]
$f = 0.03$ [mm/rev]
$v = 115$ [m/min]

Surface No. 20
$F_b = 100$ [N]
$f = 0.03$ [mm/rev]
$v = 115$ [m/min]

Surface No. 24
$F_b = 150$ [N]
$f = 0.06$ [mm/rev]
$v = 115$ [m/min]

was $\alpha = 0.05$. The results of the Shapiro-Wilk test are summarized in Table 6.

In the Shapiro-Wilk test, 36 groups were analyzed, and 24 groups out of 36 fulfilled the normality requirement with a P-value higher than the critical level at the 5% significance level. Based on these results, the ANOVA analysis cannot be carried out for all the 12 independent/dependent variable pairs without distortion of the result. The ANOVA results are summarized in Table 7. If the P-value significance level is higher than 0.05, the means of the samples are equal at the 5% significance level.

If the ANOVA results are not accepted because of the lack of normality in the data, six cases can be analyzed (decision is underlined in Table 7). The means of the axial residual stresses values are equal when the grouping factor is F_b, i.e. the burnishing force has no effect on the axial residual stress. The tangential residual stresses and the hardness values are influenced by the burnishing force, the means of the groups are considered equal. Concerning the feed rate, only the axial residual stress data can be analyzed because of the fulfilment of normality. The feed rate influences this variable, the mans are different. In the case of burnishing speed, the two residual stress variables can be analyzed. The burnishing speed has no effect on them because the means are equal.

One of the other important statistical analyses is the signal-to-noise ratio. For doing so, the integrated Taguchi method in

Table 6 SW statistics and *P*-values of the Shapiro-Wilk test

	F_b [N]	SW	P	Decision	f [mm/rev]	SW	P	Decision	v [m/min]	SW	P	Decision
Ra	50	0.926	0.440	Accept	0.03	0.707	0.002	Reject	41	0.903	0.270	Accept
	100	0.813	0.029	Reject	0.06	0.577	0.000	Reject	82	0.732	0.003	Reject
	150	0.873	0.131	Accept	0.09	0.709	0.002	Reject	115	0.767	0.009	Reject
σ-axi	50	0.916	0.363	Accept	0.03	0.963	0.834	Accept	41	0.839	0.057	Accept
	100	0.948	0.667	Accept	0.06	0.922	0.409	Accept	82	0.902	0.264	Accept
	150	0.953	0.722	Accept	0.09	0.932	0.497	Accept	115	0.919	0.386	Accept
σ-tan	50	0.920	0.390	Accept	0.03	0.824	0.038	Reject	41	0.924	0.425	Accept
	100	0.963	0.832	Accept	0.06	0.921	0.402	Accept	82	0.909	0.311	Accept
	150	0.855	0.085	Accept	0.09	0.912	0.327	Accept	115	0.865	0.109	Accept
HV 0.2	50	0.920	0.390	Accept	0.03	0.747	0.005	Reject	41	0.884	0.174	Accept
	100	0.959	0.788	Accept	0.06	0.736	0.004	Reject	82	0.779	0.012	Reject
	150	0.917	0.369	Accept	0.09	0.827	0.041	Reject	115	0.754	0.006	Reject

Table 7 ANOVA results

	F_b [N]				f [mm/rev]				v [m/min]			
	F	P	R^2	Decision	F	*P*	R^2	Decision	F	P	R^2	Decision
Ra	8.06	0.002	0.40	Different	0.69	0.512	0.05	Equal	1.12	0.342	0.09	Equal
σ-axi	2.17	0.136	0.15	<u>Equal</u>	4.45	0.023	0.27	<u>Different</u>	0.64	0.534	0.05	<u>Equal</u>
σ-tan	3.58	0.044	0.23	<u>Different</u>	1.09	0.352	0.08	Equal	1.66	0.211	0.12	<u>Equal</u>
HV 0.2	6.49	0.006	0.35	<u>Different</u>	1.5	0.243	0.11	Equal	2.07	0.149	0.15	Equal

The underlined decisions are accepted ANOVA results

the Minitab 20 software was used. The S/N ratio gives an indication of the optimum factor settings that reduce noise sensitivity. A higher signal-to-noise ratio (S/N) indicates a more effective setting for the control factor that reduces the impact of the noise components. For this study, the different patterns of responses were converted into S/N ratios, which were then used to characterize their quality. The S/N ratios were differentiated by "smaller is better" for the surface roughness results and by "larger is better" for the other three responses, taking into account that the absolute values of stresses were used in the evaluations, and the "larger" was considered with the higher values of compressive stresses.

For the whole responses, S/N ratios are summarized in Table 8. Whereas their corresponding main effects' plots are shown in Fig. 11. For the surface roughness, Figure a shows that the higher impact is for the burnishing force, followed by the velocity, and finally by the burnishing feed. According to the results, the best surface roughness could be achieved using the second force, with an influential weight of 56%, and the first velocity and feed, with weights of 23.4% and 20.6%, respectively. It is worth mentioning that these weights were calculated from the results of the response table for the S/N ratios of each response. Concerning the axial residual stresses (Figure b), the main effect is for the burnishing feed, then for the force, and finally for the speed. The best combination of the three factors could

be achieved when using the second burnishing force, the second feed, and the first velocity, at weights of 46.4%, 33.8, and 19.8, respectively. Figure c shows the results of stresses in the tangential direction. The most influential factor on stresses is the burnishing force, followed by the speed, and the feed has the lowest impact. According to the analysis, the best results could be achieved when the second force and feed were used along with the first speed. In this case, 49.6% is the weight of force, 28.1% is for the speed, and 22.2% is for the feed. Finally, for the microhardness (Figure d), the burnishing force has the highest effect, followed by the speed, and finally the feed. The best pairing of parameters that gives the preferable microhardness is utilizing the third force, the second speed, and the first feed. In this case, their weights will be 43.1%, 30.1%, and 26.8%, respectively.

For the purpose of summarizing the results of the S/N ratios analysis, Table 9 shows the first, second, and third influential factors on the responses, the optimal combinations of the three parameters and their levels, and the weight of each one in that combination. It should be noticed that the most effective parameter is the burnishing force, followed by the burnishing speed, and finally the feed, which has the lowest effect on the responses. Moreover, the last three columns in the table show the values of the responses as predicted from the analysis, the corresponding highest experimental values, and the percentage of error between them, respectively. As can be seen, the percentage of

Table 8 Influencing factors and the signal-to-noise ratios for each response

Surf. no	F_b [N]	f [mm/rev]	v [m/min]	Ra [µm]	S/N ratio	σ-axi [MPa]	S/N ratio	σ-tan [MPa]	S/N ratio	HV 0.2	S/N ratio
1	50	0.03	41	0.134	17.5	1032	60.3	542	54.7	721	57.2
2	100			0.151	16.4	1167	61.3	607	55.7	719	57.1
3	150			0.204	13.8	1313	62.4	623	55.9	778	57.8
4	50	0.06		0.167	15.5	1011	60.1	510	54.2	675	56.6
5	100			0.172	15.3	1033	60.3	623	55.9	707	57.0
6	150			0.201	13.9	1130	61.1	660	56.4	661	56.4
7	50	0.09		0.202	13.9	987	59.9	447	53.0	675	56.6
8	100			0.147	16.7	964	59.7	551	54.8	652	56.3
9	150			0.159	16.0	1005	60.0	641	56.1	660	56.4
10	50	0.03	82	0.144	16.8	986	59.9	511	54.2	698	56.9
11	100			0.154	16.2	1157	61.3	503	54.0	703	56.9
12	150			0.311	10.1	968	59.7	304	49.7	950	59.6
13	50	0.06		0.186	14.6	982	59.8	448	53.0	667	56.5
14	100			0.175	15.1	1160	61.3	579	55.3	735	57.3
15	150			0.533	5.5	1134	61.1	289	49.2	939	59.5
16	50	0.09		0.144	16.8	896	59.0	488	53.8	698	56.9
17	100			0.137	17.3	980	59.8	634	56.0	700	56.9
18	150			0.603	4.4	757	57.6	311	49.9	816	58.2
19	50	0.03	115	0.125	18.1	905	59.1	500	54.0	696	56.9
20	100			0.131	17.7	1203	61.6	633	56.0	723	57.2
21	150			0.475	6.5	843	58.5	133	42.5	891	59.0
22	50	0.06		0.191	14.4	1068	60.6	603	55.6	713	57.1
23	100			0.134	17.5	1285	62.2	725	57.2	747	57.5
24	150			0.129	17.8	1278	62.1	706	57.0	734	57.3
25	50	0.09		0.252	12.0	1013	60.1	475	53.5	677	56.6
26	100			0.234	12.6	1084	60.7	563	55.0	688	56.8
27	150			0.621	4.1	873	58.8	181	45.2	740	57.4

agreement was 100% for the case microhardness, 86% for tangential stresses, and around 79% for the surface roughness and the axial residual stresses. This variance comes from the complexity of the burnishing process and the high number of factors that influence the process, like the different applied burnishing parameters, vibration, heat generation, lubrication, etc.

As may be observed, there is, to a large extent, agreement between the previous observations and the results obtained from this analysis. As was mentioned before, the first level of the force (50 N) was not high enough to decrease the roughness of the burnished surface, induce high residual stresses, or increase its microhardness. Therefore, it was excluded from the table. Also, the higher level of force (150 N) was just good enough to increase the microhardness but not to improve the other responses. Additionally, the higher values of feed and speed do not exist in the table.

Comparing the results of ANOVA and S/N ratio analysis, the followings can be concluded.

- Because of the lack of normality, ANOVA cannot be considered reliably in the case of the *Ra* parameter.

- Significant differences were obtained in the axial residual stress values at different feed rates by ANOVA, and it was confirmed by the S/N ration analysis by the highest weight of the feed rate (46.4%).
- In the cases of the tangential residual stress and the HV 0.2 hardness, the highest differences between the means were obtained at different burnishing forces based on the results of ANOVA. This was confirmed by the S/N ratio analysis by 49.6 and 43.1% weights.

If the analyzed parameters (dependent variable, e.g., *Ra*) are grouped based on the three levels of a factor (an independent variable), nine groups can be obtained for the 27 data points, with nine data points in each group. When the data points of a parameter are grouped based on the levels of a factor that influences the parameter, the standard deviations of the groups are lower than those obtained by grouping based on a non-influencing factor. The reason for this is that, in the latter case, the groups incorporate values influenced by the former factor.
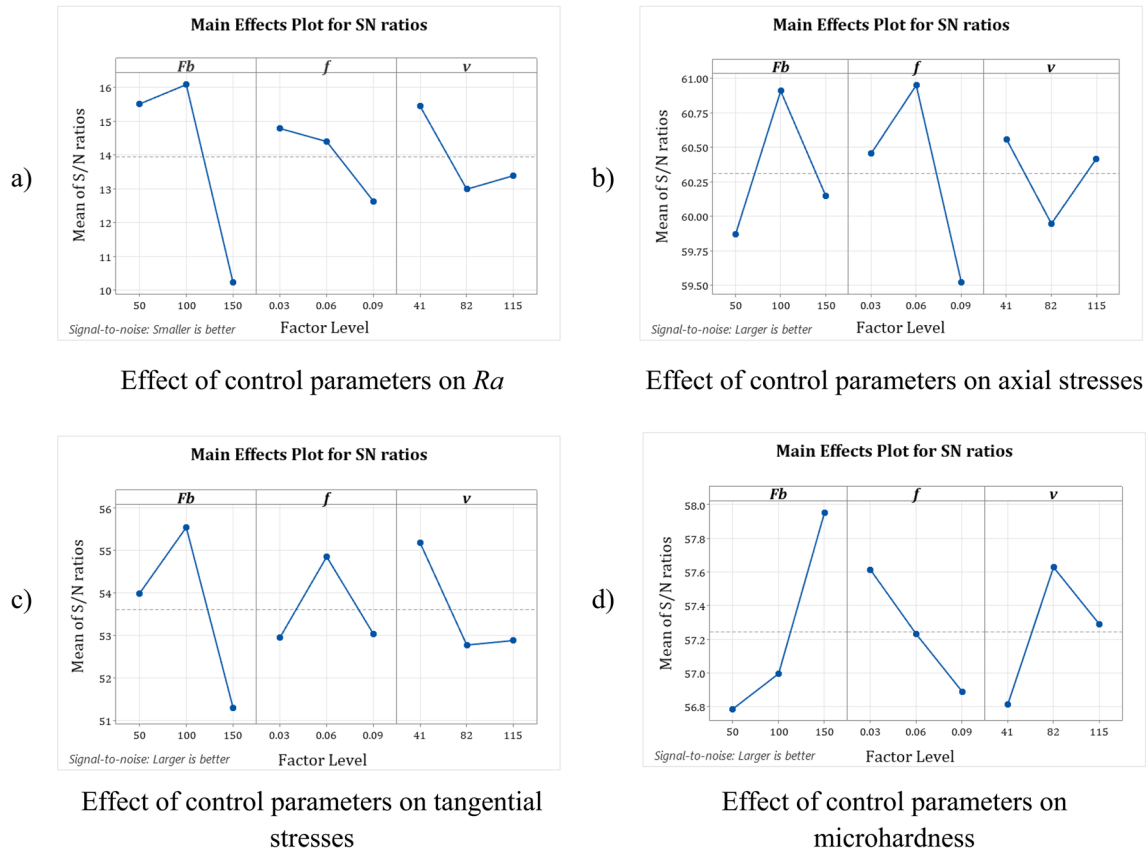
Effect of control parameters on *Ra*

Effect of control parameters on axial stresses

Effect of control parameters on tangential stresses

Effect of control parameters on microhardness

Fig. 11 Effect of control parameters on the different responses

Table 9 Summary of the S/N ratios analysis

	First factor			Second factor			Third factor			S/N	Exp	% Err.
	Factor	Level	Weight [%]	Factor	Level	Weight [%]	Factor	Level	Weight [%]			
Ra	F_b	2	56	v	1	23.4	f	1	20.6	0.125	0.151	20.8
σ-axi	f	2	46.4	F_b	2	33.8	v	1	19.8	1313	1033	21.3
σ-tan	F_b	2	49.6	v	1	28.1	f	2	22.2	725	623	14.1
HV 0.2	F_b	3	43.1	v	2	30.1	f	1	26.9	950	950	0.0

The means of the standard deviations of each factor level are summarized in Table 10. For example, the mean of the standard deviations of the three groups of the *Ra* formed based on the levels of the burnishing speed is 0.128 μm. In the case of *Ra*, the strongest influencing factor is the burnishing force. The standard deviations of the three groups formed based on F_b are the lowest. This is valid for the tangential residual stresses and the HV 0.2 hardness. This finding confirms those of the S/N ratio analysis. In the case of the axial residual stresses, the two lowest values were obtained for f and F_b. This finding partly confirms those of the S/N ratio analysis.

For the quantification of the effects, response functions were constructed for the dependent variables. The quadratic

Table 10 Means of standard deviations of the responses

Factor	*Ra*	σ-axi	σ-tan	HV 0.2
v	0.128	137.7	136.0	71.0
f	0.145	119.8	150.9	75.8
F_b	0.090	118.95	112.8	52.3

form was used because it incorporates the effects of interactions among the independent variables (burnishing parameters) and is more exact than the linear or quasilinear types [41]. The constant parameters of the functions can provide information about which dependent variables are influenced more than others by a certain dependent variable (Eqs. 2–5).

For example, the burnishing force decreases the four dependent variable values (a negative constant in each case). The absolute value is the highest in the case of the tangential residual stress and the lowest in the case of the Ra roughness, which indicates that this force has a larger effect on the tangential residual stress. Due to the negative influencing directions, the weighting of the influencing parameters cannot be carried out.

$$Ra = 0.5739 - 0.0096F_b - 6.0993f + 0.0022v$$
$$+ 0F_b^2 + 34.074f^2 + 0v^2 + 0.0110F_bf + 0F_bv \quad (2)$$
$$+ 0.0271fv$$

$$\sigma - axi = -533.36 - 11.901F_b - 12,395f + 8.0669v + 0.0419F_b^2$$
$$+ 125,247f^2 - 0.0470v^2 + 25.667F_bf + 0.0191F_bv - 41.871fv \quad (3)$$

$$\sigma - tan = 18.063 - 13.101F_b - 10,222f + 6.6199v + 0.0548F_b^2$$
$$+ 101,173f^2 - 0.0622v^2 - 12.000F_bf + 0.0456F_bv - 7.5363fv \quad (4)$$

$$HV0.2 = 577.51 - 1.6866F_b + 412.96f + 4.9822v + 0.0142F_b^2$$
$$+ 1790.1f^2 - 0.0376v^2 - 18.778F_bf \quad (5)$$
$$+ 0.0128F_bv + 2.3810fv$$

To analyze the strengths of relationships between the process parameters and the dependent variables, correlation analysis was carried out. The correlation coefficient provides information about the strength and direction of the relationship between two variables, but it provides no information about which variable influences which. However, it is logical that the process parameters can influence the dependent variables (e.g., Ra) and not vice versa. In Table 11, the correlations between the dependent and independent variables are summarized. The interactions (according to the ones incorporated in the response functions) were also considered. No strong correlation ($r > 0.7$) was obtained in the analysis, and a medium relationship ($0.3 < r < 0.7$) was obtained only in 13 cases. This means that no inevitably strong relationships were obtained.

Based on these statistical results, clear optimization is not possible without distortion. The reason for this is that in the case of diamond burnishing, the response variables are not significantly sensitive for all the process parameters, as obtained from the statistical results. However, optimization can be realized only for a single dependent variable at a time because it can be observed that when one decreases, another decreases or shows randomness. In the case of concrete industrial specifications, however, the possible or best values can be found without using the statistical results.

4 Conclusion

The current research work describes the influence of three of the main parameters of the slide diamond burnishing process on surface roughness, surface residual stresses, and microhardness. Burnishing was conducted on 42CrMo4 hard-turned steel bars. The investigated parameters were burnishing speed, feed, and force. The experimental results have shown that a significant reduction in the surface roughness was achieved, besides introducing high compressive residual stresses in the axial and tangential directions to a considerable depth of about 135 μm. The microhardness of the surfaces was also improved and reached 51% improvement in some samples. After investigating the effects of the three burnishing parameters simultaneously, results exhibited that it is not sufficient to study the effect of changing only one parameter while keeping the others unchanged. Results showed that the influence of one parameter is highly affected by the range in which the other parameters have been applied. Therefore, the optimal burnishing parameters that gave the best results were specified. Using these parameters, a smaller surface roughness was obtained than what is achievable by grinding. Furthermore, in contrast with grinding, favorable compressive stresses were introduced into the surface regions of the treated specimen. Finally, the effect of the burnishing feed and force on the surface topography, morphology, and microstructure was evaluated for some samples. The influence of those parameters was obvious on the surfaces. Results revealed that the intensity of the burnishing force had a major impact on the deformation rate and depth of the burnished layer. ANOVA, S/N ratio, and standard deviation analysis were carried out to determine the main burnishing factors that influence the roughness, residual stresses, and hardness responses. It was found that the main influencing factor of Ra roughness, the tangential residual stresses, and the HV 0.2 hardness is the burnishing force, and that of the axial residual stresses is the feed rate. Beyond that, the order among the strengths of influences was also determined by the S/N ratio analysis. The results were confirmed by the analysis of standard deviations. Response functions were constructed

Table 11 Correlations between the dependent and the independent variables

Response	F_b	f	v	F_b^2	f^2	v^2	F_bf	F_bv	fv
Ra	0.53	0.21	0.25	0.57	0.22	0.22	0.52	0.60	0.35
σ-axi	−0.14	0.34	0.04	−0.09	0.39	0.01	0.19	−0.02	0.21
σ-tan	0.21	0.02	0.23	0.27	0.06	0.19	0.13	0.39	0.15
HV 0.2	0.55	−0.33	0.23	0.58	−0.33	0.19	0.08	0.59	−0.08

for the measured data, and the correlation coefficients were calculated for the burnishing parameters, and their interactions confirmed the results of strength of influence obtained by the other methods.

Data availability Upon request, the corresponding author will provide access to all relevant data and materials used in generating the results presented in this work.

Code availability Not applicable.

Declarations

Ethics approval The authors confirm that there are no ethical concerns with this study.

Consent to participate All authors agree to be included in and make contributions to this study.

Consent for publication The research can be published with the agreement of all authors. No concerns about plagiarism or copyright infringement exist with this study.

Competing interests In terms of competing interests, the authors report none.

References

1. Arsalani M, Razfar MR, Abdullah A, Khajehzadeh M (2021) Fatigue behavior improvement of hardened parts using sequential hard turning, grinding, and ball burnishing operations. Proc Inst Mech Eng Part L J Mater Des Appl 235:87–99

2. Davim JP (2011) Machining of hard materials. London, Springer

3. Stephenson DA, Agapiou JS (2018) Metal cutting theory and practice. CRC Press

4. Hua J, Shivpuri R, Cheng X et al (2005) Effect of feed rate, workpiece hardness and cutting edge on subsurface residual stress in the hard turning of bearing steel using chamfer + hone cutting edge geometry. Mater Sci Eng A 394:238–248. https://doi.org/10.1016/j.msea.2004.11.011

5. Kluz R, Trzepiecinski T, Bucior M, Antosz K (2021) Modelling of the effect of slide burnishing on the surface roughness of 42CrMo4 steel shafts. Lect Notes Mech Eng 14:415–424. https://doi.org/10.1007/978-3-030-77719-7_41

6. Tobola D, Czechowski K, Laszkiewicz-Lukasik J, Cygan S (2015) Burnishing of PM tool steels using diamond composite material. Euro PM2015 – Secondary Operations. European PM Conference Proceedings, p 1

7. Líska K, Kodácsy J, Líska J (2012) Investigation of the microgeometry after hard turning and diamond burnishing. Adv Mater Res 472–475:902–907

8. Toboła D, Brostow W, Czechowski K et al (2015) Structure and properties of burnished and nitrided AISI D2 tool steel. Mater Sci 21:511–516

9. Brostow W, Czechowski K, Polowski W et al (2013) Slide diamond burnishing of tool steels with adhesive coatings and diffusion layers. Mater Res Innov 17:269–277

10. Huuki J, Laakso SVA (2017) Surface improvement of shafts by the diamond burnishing and ultrasonic burnishing techniques. Int J Mach Mach Mater 19:246–259

11. Okada M, Shinya M, Matsubara H et al (2017) Development and characterization of diamond tip burnishing with a rotary tool. J Mater Process Technol 244:106–115

12. Maximov JT, Duncheva GV, Anchev AP et al (2020) Improvement in fatigue strength of 41Cr4 steel through slide diamond burnishing. J Brazilian Soc Mech Sci Eng 42:1–20

13. Konefal K, Korzynski M, Byczkowska Z, Korzynska K (2013) Improved corrosion resistance of stainless steel X6CrNiMoTi17-12-2 by slide diamond burnishing. J Mater Process Technol 213:1997–2004

14. Korzynski M, Lubas J, Swirad S, Dudek K (2011) Surface layer characteristics due to slide diamond burnishing with a cylindrical-ended tool. J Mater Process Technol 211:84–94

15. Revankar GD, Shetty R, Rao SS, Gaitonde VN (2017) Wear resistance enhancement of titanium alloy (Ti–6Al–4V) by ball burnishing process. J Mater Res Technol 6:13–32

16. Toboła D, Brostow W, Czechowski K, Rusek P (2017) Improvement of wear resistance of some cold working tool steels. Wear 382:29–39

17. Maximov JT, Duncheva GV, Anchev AP, Ichkova MD (2019) Slide burnishing—review and prospects. Int J Adv Manuf Technol 104:785–801

18. Łabanowski J, Ossowska A (2006) Influence of burnishing on stress corrosion cracking susceptibility of duplex steel. Work 5:7

19. Boguslaev VA, Yatsenko VK, Yakovlev VG et al (2008) The effect of diamond burnishing on structure and properties of detonation-gas coatings on gas-turbine engine parts. Met Sci Heat Treat 50:44–48

20. Korzynski M, Pacana A, Cwanek J (2009) Fatigue strength of chromium coated elements and possibility of its improvement with slide diamond burnishing. Surf Coatings Technol 203:1670–1676

21. Hankare AV, Sapkal AA, Dounde AA (2017) Effect of diamond burnishing process on surface roughness of AISI 4140 alloy steel. J Adv Sci Technol 13:405–410

22. Korzynski M (2007) Modeling and experimental validation of the force–surface roughness relation for smoothing burnishing with a spherical tool. Int J Mach Tools Manuf 47:1956–1964

23. Świrad S (2011) The surface texture analysis after sliding burnishing with cylindrical elements. Wear 271:576–581

24. Xu Q, Liu Y, Lu H et al (2021) Surface integrity and corrosion resistance of 42CrMo4 high-strength steel strengthened by hard turning. Materials (Basel) 14:6995

25. Xu Q, Zhao J, Ai X (2017) Cutting performance of tools made of different materials in the machining of 42CrMo4 high-strength steel: a comparative study. Int J Adv Manuf Technol 93:2061–2069

26. Callister WD, Rethwisch DG (2018) Materials science and engineering: an introduction. Wiley, New York

27. Chandler H (1994) Heat treater's guide: practices and procedures for irons and steels. (2nd ed.). ASM International, USA

28. Nestler A, Schubert A (2015) Effect of machining parameters on surface properties in slide diamond burnishing of aluminium matrix composites. Mater Today Proc 2:S156–S161

29. Kuznetsov VP, Tarasov SY, Dmitriev AI (2015) Nanostructuring burnishing and subsurface shear instability. J Mater Process Technol 217:327–335

30. Shirsat U, Ahuja B, Dhuttargaon M (2017) Effect of burnishing parameters on surface finish. J Inst Eng Ser C 98:431–436

31. Saldaña-Robles A, Plascencia-Mora H, Aguilera-Gómez E et al (2018) Influence of ball-burnishing on roughness, hardness and corrosion resistance of AISI 1045 steel. Surf Coatings Technol 339:191–198

32. Maximov JT, Anchev AP, Duncheva GV et al (2017) Influence of the process parameters on the surface roughness, micro-hardness, and residual stresses in slide burnishing of high-strength aluminum alloys. J Brazilian Soc Mech Sci Eng 39:3067–3078

33. Kalpakjian S, Schmid SR, Sekar KS (2021) Manufacturing engineering and technology. (7th ed.). Pearson Education Limited, United Kingdom

34. Ibrahim AA (2008) An investigation into ball burnishing process of carbon steel on a lathe. In: Proceedings of Al-Azhar engineering tenth international conference, Cairo, Egypt

35. Kim W, Kawai K, Koyama H, Miyazaki D (2007) Fatigue strength and residual stress of groove-rolled products. J Mater Process Technol 194:46–51

36. McClung RC (2007) A literature survey on the stability and significance of residual stresses during fatigue. Fatigue Fract Eng Mater Struct 30:173–205

37. Toboła D, Rusek P, Czechowski K et al (2015) New indicators of burnished surface evaluation–reasons of application. Metrol Meas Syst 22:263–274

38. Toboła D, Morgiel J, Maj Ł (2020) TEM analysis of surface layer of Ti-6Al-4V ELI alloy after slide burnishing and low-temperature gas nitriding. Appl Surf Sci 515:145942

39. Roy R, Ghosh SK, Kaisar TI et al (2022) Multi-response optimization of surface grinding process parameters of AISI 4140 alloy steel using response surface methodology and desirability function under dry and wet conditions. Coatings 12:104

40. da Silva Campos PH, de Carvalho PV, de Carvalho Gonçalves ED et al (2019) Optimizing production in machining of hardened steels using response surface methodology. Acta Sci Technol 41:e38091–e38091

41. Balanou M, Karmiris-Obratański P, Leszczyńska-Madej B et al (2021) Investigation of surface modification of 60CrMoV18-5 steel by EDM with Cu-ZrO2 powder metallurgy green compact electrode. Machines 9:268